12 Simulations of the Variability of the Tropical Atlantic

M.J.ORTIZ BEVIA, W. CABOS NARVAEZ
Departamento de Fisica, Universidad de Alcala de Henares, Apdo 20, 28880 Alcala de Henares, Madrid, Spain.

J. M. OBERHUBER
DKRZ, Bundestrasse 55, D-20146 Hamburg.

12.1 Introduction

In a number of observational studies, the seasonal as well as the interannual variability in the tropical Atlantic has been analysed (Arnault, 1987; Houghton, 1993; Weingartner and Weisberger, 1987, 1991; Servain, 1993). The seasonal cycle of the tropical Atlantic ocean has been successfully simulated by simple and more complete general circulation ocean models (see the review by Duchene and Frankignoul (1990)). Details of this circulation specially difficult to simulate are the subject of recent studies with high resolution models (Johns et al. (1990), Schott and Boening (1991)).

The most important features of the interannual variability of the tropical Atlantic are the episodic warmings and coolings of the temperatures in the Gulf of Guinea. These are characterized by the Gulf of Guinea index (hereinafter GG index), shown in Fig. 12.1. This index was produced by averaging the SST anomalies, previously smoothed with a three points running mean, to the region (20W - 10E, 3N - 12S) (Servain (1993)). In Fig. 12.1 we also show the Niño3 index, built also form SST anomalies, that were similarly smoothed and averaged to the region (150W - 90W, 5S - 5N). The observed Atlantic warming events take place every years, and never reach more than 1.8° K.

With respect to the Pacific case, the intensity is reduced and the maxima occur more towards the center of the basin. The relationships with ENSO events have been investigated in early observational studies (Wright, 1987). The correlation between both indices is significant, with a maximum value of 0.65, obtained with the GG index lagging the Niño3 index by three months. But there were Atlantic warmings not preceded by any ENSO signal. Precipitations in North-East Brazil are heavily correlated with the GG index, while only weakly with El Niño, although the region is nearer to the coast of Peru than to the Gulf of Guinea.

At seasonal time scales, the circulation in the tropical Atlantic has some traits in common with those of the other tropical oceans, as for instance, the equatorial system of currents or the eastern basin upwelling in summer and fall of the northern hemisphere. Other effects, as the mainly meridional displacement of the Intertropi-

cal Convergence Zone (ITCZ) are particular of this basin. While many of the features of the seasonal Atlantic variability are well documented and explained in the literature (see for instance Philander and Pacanowski, 1986), the mechanism that determines the interannual variability and its relationships with ENSO are currently being discussed.

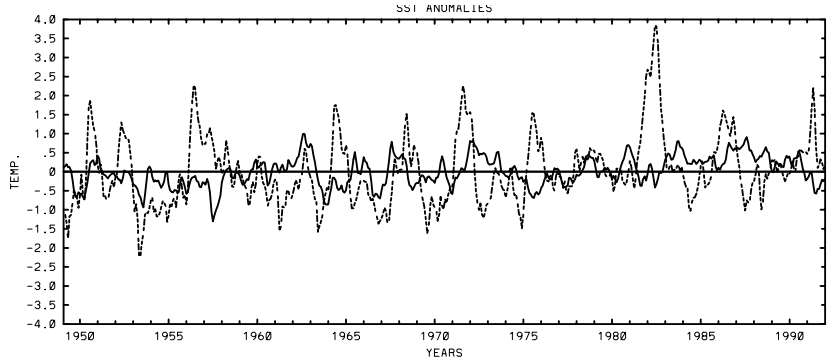

Fig. 12.1 The GG Index (dashed line), from 1950 to 1992 against the Niño3 index (solid line), for the same years.

In the last years there has been an increased interest in the interannual variability of the Atlantic basin and the tropical Atlantic has received renewed attention. Because of the poor coverage, specially of subsurface data, the knowledge of this variability through observations is necessarily limited. Model simulations could be very valuable to understand the physical interactions that determine it. In intermediate coupled models of the equatorial Atlantic (Zebiak, 1993), the spatial and temporal characteristics of the equatorial warmings are explained by a coupled mode. In these simulations, there is another coupled mode, with a decadal time scale of variability, and apparently not related to the Gulf of Guinea warmings, known as the dipole mode (Ping Chang et al., 1997).

Some of the modeling studies focus on the relationships between ENSO and the Atlantic events. For instance, Delecluse et al. (1994) use an oceanic general circulation model (OGCM) forced with the response of an atmospheric general circulation model to observed SST, and Latif and Barnett (1995), a fully coupled general circulation model. Links between the Atlantic and Pacific warmings have also been the aim of recent observational studies (Curtis and Hastenrath (1995), Wagner (1996)). In both of these studies, there is a new stress on the importance of the wind anomalies in the north tropical Atlantic in controlling the northward SST gradient. This gradient in turn, has a significant part in the GG index variability (Cabos et al., 1998). The mechanisms of interaction between ENSO and the tropical Atlantic are traced in Endfield and Mayer (1997) to a weakening of the northern trades and the following sea surface temperature warming, persistent although weak. North of this

region, the enhancement of the subtropical gyre detected is unrelated to any SST local anomaly.

Only modeling studies with coupled general circulation models give a simulation of the ocean-atmosphere interactions that is exhaustive and free from observational errors, but simulations of particular events, obtained by forcing an OGCM with atmospheric observations, can also be valuable. In the case of the tropical Atlantic, there are only two datasets of observations covering an extended period: the ECMWF analysis and the subjectively analyzed observations by Servain et Legler (1996). In a series of papers, Huang and others (Carton and Huang, 1994; Huang et al., 1995; Huang and Shukla, 1997) have recently used both of them as forcing of an OGCM to simulate the equatorial Atlantic variability for the years 1980-1989.

In the present work we also simulate the interannual equatorial Atlantic variability by forcing an OGCM with atmospheric observations. In order to understand the generation of the events, we focus on the features that are common to several of them. The events compared are those simulated in the decade 1980-1989, where three warmings (1981, 1984 and 1988) took place. In the first of our simulations, hereafter referred to as E1, where the forcing data came from the ECMWF analysis, the 1984 and 1988 events were successfully reproduced, while the 1981 warming was missed. To investigate the reasons of this failure, we have carried out our second simulation (run S1), where the Servain et al. data were used for the anomalous atmospheric forcing. Two other simulations (E2 and S2) were intended to test the influence of the mid-latitude anomalies in the generation of the events.

Coupled model studies have shown that the “heat content”, that is, the thermal energy stored in the ocean upper layers, is the optimal variable to monitor the generation of the anomalous warmings of the tropical oceans (Chao and Philander (1993), Latif and Graham (1992)). Nevertheless, the onset stage of the warmings has been also related to anomalies in other surface variables, like mixed layer velocity convergence (Latif and Graham, 1992; Latif et al., 1996). Can the anomalies of the surface variables be related to the heat content anomalies in a simple way? To check this point, we reduce the evolution of the heat content anomalous field to those of a few modes, and, through simple statistical modeling, we try to connect them with other surface variables, like mixed layer velocities, or wind stresses.

The structure of the paper is as follows. The simulation of the seasonal variability is described in section 12.2, where details of the model layout and the forcing used for this simulation are also given. In section 12.3, different simulations for the period 1980-1989 are described, and its interannual variability, represented by the GG index, is compared. In this section, we also include a description of a coupled run (OPYC-T42), whose interannual variability in the tropical Atlantic will be used to test the generality of the analysis of the forced simulations. In section 12.4, we study the onset and evolution of the events in different simulations, through the analysis of the anomalous heat content field. In section 12.5, we include details of the systematic statistical analysis followed in Cabos et al. (1998) to relate the evolution in time of the anomalous heat content to those of the anomalies of other oce-

anic variables or of the forcing fields. The results presented through this paper are discussed in section 12.6.

12.2 Simulation of the seasonal variability

Our simulation of the seasonal cycle is satisfactory (Cabos et al. (1998)), and similar to the one reported in Carton Huang (1994), and in Huang et al. (1995). The model used in this work is an updated version of the model developed by Oberhuber (1993a). An updated summary can be found in the Appendix of Cabos et al. (1998). It consists in a number of isopycnal ocean layers fully coupled to a surface bulk mixed layer model, that in turn is coupled to a sea-ice model. Isopycnal models use Lagrangian coordinates in the vertical, in contrast to level models, where the grid points are at fixed depth levels. The model solves the full primitive equations for mass, mass flux, temperature and salinity in spherical geometry with a realistic equation of state. The layers' interchange is due to diapycnal mixing and convection. The interior ocean is coupled to the mixed layer through the entrainment/detrainment processes. A potential vorticity and enstrophy conserving scheme is implemented. In the horizontal, the equations are discretized on an Arakawa B-grid. A time integration scheme consisting of a semi-implicit scheme combined with a predictor-corrector technique is used in order to achieve large time steps. Table 12.1 includes the values of some of the relevant parameters adopted in the present simulation.

Parameter	Typical Value	Description
m_0	0.5	Coefficient for wind stirring
δt	12 hr	Simulation Time Step
h_B	20m	Solar radiation Penetration depth
μ	1.67	Ekman layer constant
c_r	0.0012	Surface Drag Coefficient

Table 12.1 Model parameters, typical value and description

The model domain covers 56°S to 65°N, and 80°W to 20°E. The grid varies zonally from 2.0° to 1.5° and meridionally from 2.6° to 0.5°. The center of the zonal focus is in the GG, while the meridional one is on the equator. The model has eleven layers, the time step is half a day and the model uses non-slip boundary conditions along the coasts. The domain is open to the north and south.

The main difference between the present version of the model and the one used in others simulations, as for instance by Miller et al. (1994), consists in the way the boundary conditions in the open ocean are imposed. For the present simulation we have used a new version of the model that incorporates an open boundary formulation, due to Kauker and Oberhuber (1996). The main point of this formulation is

that on the boundary the pressure is imposed but near it, the flow is fully computed and not prescribed at all. Boundary conditions, namely the layers thicknesses, potential temperatures and salinities are taken from the output of a global OGCM of higher resolution (a global version of OPYC at horizontal resolution corresponding to grid of the T106, forced with climatological winds and fluxes). In this way, the boundary values are interpolated only horizontally, avoiding the errors introduced by interpolating in the vertical. The barotropic part of the sea level at the boundaries was estimated from the barotropic transport of this global run using the geostrophic approximation. Nevertheless, because of the inclusion of two open boundaries, one is left with the problem of determining the differences between mean sea levels at these. In this case, the value of this difference in the global model can be taken only as a first indication. Because of the disparities in the global and regional model resolution are conveyed into their physics, this difference in mean sea level must be finally tuned.

The data sets required to force the model are air temperature, relative humidity, cloudiness, wind stress, the time averaged absolute wind speed and its standard deviation, and surface salinity. The wind stress data are basically the climatology of the ECMWF analysis from 1980 to 1989, corrected at the equator with the Hellermann-Rosenstein climatology. The other atmospheric forcing data required for the forcing come basically from COADS, although other global data sets were also used. The model was forced with heat fluxes derived from observations according to Oberhuber (1988) plus a relaxation to the climatology of the observed SST.

$$Q_s = Q_{obs} - \left(\frac{dQ}{dT}\right)_{obs} (T_{obs} - T_S) \qquad (12.1)$$

where T_{obs} and T_S are the observed and simulated climatological SST. The relaxation coefficients $(dQ/dT)_{obs}$ are also computed following Oberhuber (1988). During the last year of the spinup, the daily values of Q_s were saved, and used afterwards as the forcing in the anomalous run.

We can characterize the Carton and Huang (1994), and Huang et al. (1995) simulation in terms of its vertical discretization of the model (fixed levels), the physical parameterization used, the model domain and layout and the parameterization of the heat fluxes. Only the winds stresses are common to our simulation of the tropical Atlantic. In the case of the wind forcing, the differences can (they include a high frequency component) be considered small. And nevertheless both models are successful at simulating the tropical Atlantic variability at two different (annual and interannual) time scales.

Observations show that the ITCZ is nearer the Gulf of Mexico in September, in March-April it is nearest to the equator and at its most eastern position. Sea surface temperatures (hereinafter SST) in the east reach then its maximum value. All the surface currents except the North Brazil current are weak and the zonal slope of the thermocline is almost horizontal. In May, as the ITCZ moves north, the intensification of the south trades is followed by a strengthening of the South Equatorial Current. Due to intense upwelling, the thermocline shoals in the east, a strong North

Equatorial Countercurrent is observed, and measurements show that an undercurrent also exits. SST reach its minimum value in the western part of the basin in July and a month later in the Gulf of Guinea. The SST errors of our simulation of the seasonal cycle, computed by subtracting the climatological monthly mean from the AMIP (Atmospheric Models Intercomparison Project) from the simulated SST are below 1° C even in the critical months (June-July-August). The seasonal evolution of the simulated currents is also captured. The error in the simulated magnitude of the currents is roughly lower than 20% in most of the domain (Richardson and Reverdin, 1987). For instance, for the North Brazil current, the estimated value is below 86 cm/s while observations show maximum values of 110 cm/s at some months. Other magnitudes like mixed layer depth or the heat content have reasonable spatial structure and values. A more detailed account can be found in Cabos et al.(1998).

12.3 The simulation E1 of the interannual variability.

Using the last year of the spinup as initial state, the model was forced with wind stresses from the ECMWF analysis for the period 1980-1989. The heat fluxes were obtained from the last year of the spinup plus a relaxation to the simulated climatology given by the expression

$$Q_s = Q_{obs} - \left(\frac{\overline{dQ}}{dt}\right)(T_{obs} - T_S) \qquad (12.2)$$

where T_a is the SST obtained in this experiment and T_S the simulated SST climatology from the last year of the spinup and $(\overline{dQ/dT}) = 0.3(dQ/dT)_{obs}$. The 0.3 is a tuning factor to obtain anomalies of the order of magnitude than the observed ones.

In Fig. 12.2a we show values of the Atlantic index simulated (dashed line) with our ocean model and the observed one (thin line). We see that the model captures quite well the warming events of 1984 and 1988 but the 1981 event is simulated as one of cooling. In our Fig. 12.3 the peak phase of the simulated warmings (middle row) is compared with observations (top). The equatorial character of the simulated warming is a trait shared with Huang et al. (1995), as well as the higher values of the anomalies with respect to observations. From a comparison month by month of the observed and simulated 1988 event (not shown) it can be seen that the starting of the episodes is well modeled. Later, when the anomalies extend to the tropics along the African coast the model does not perform well, although for the right season (winter 1989) it reproduces the cooling that closes the event.

The evolution of the cooling events (observed and simulated) compares well with the reverse of the warming events (observed and simulated respectively): the modeled cooling also anticipates the observed one. An interesting feature, common to the Huang et al. (1995) simulation and ours, is the misrepresentation of the 1981 event. This common trait supports Huang et al. (1995) conclusion that a trend in the

(a)

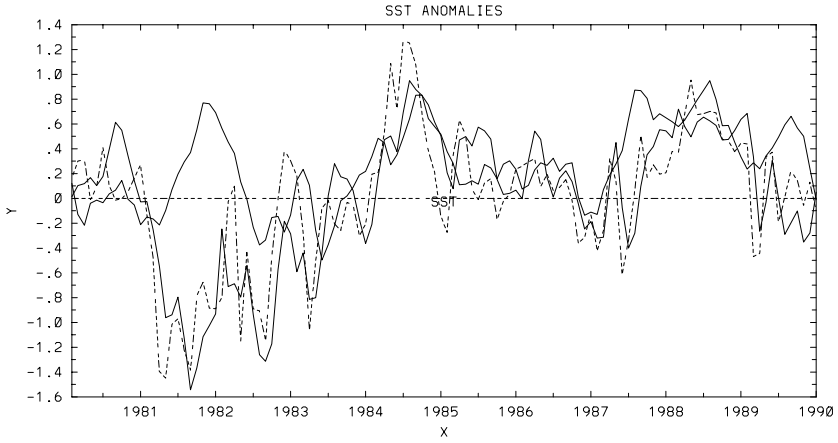

Fig. 12.2 (a) The thin continuous line represent the observed GG Index. The dashed line, the Index simulated with the E climatology and the E anomalous stresses for all the domain (run E1). The thick continuous line, the Index simulated with the E anomalous stresses only in the tropical band, superimposed on the S climatology (run E2).

(b)

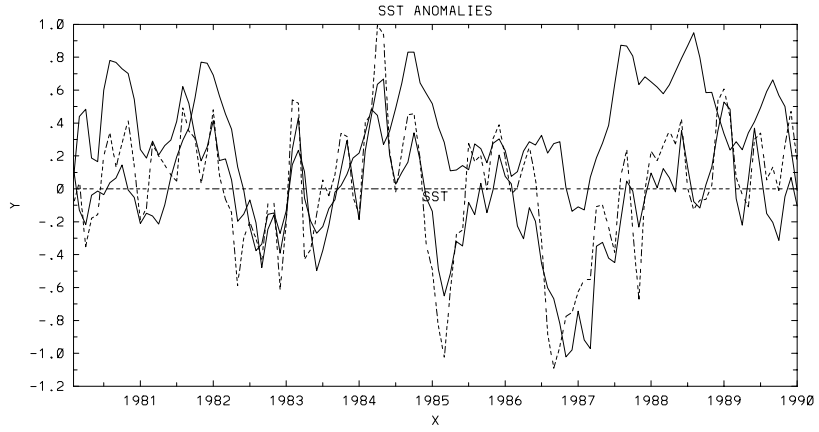

Figure 12.2 (continued) (b) The thin continuous line represent the observed GG Index. The dashed line, the Index simulated with the S climatology, the S anomalous stresses in the tropical band and the E anomalous stresses for the rest of the domain (run S1). The thick continuous line, the Index simulated with the S anomalous stresses only in the tropical band, superimposed on the S climatology (run S2).

ECMWF winds is responsible for this failure. The magnitude of the simulated SST anomalies (too big) can also have a role in this mismatch between simulated and observed world.

12.4 Sensitivity experiments: simulations S1, S2 and E2.

In a series of sensitivity experiments, additional runs for the same period and using the same stresses were performed. For instance, different values for the drag constant used for the wind stresses were chosen. Also the values of the restoring condition to the climatology used in the anomalous heat fluxes was systematically varied. Values for the drag constant do influence the magnitude of the anomalies, down to a threshold below which the interannual variability was not successfully simulated. Small changes in the feedback-time of the restoring condition does not improve the simulation of the whole period, while one of the warming events is better reproduced, the simulation of the other worsens. Three additional simulations of the interannual variability for this region were devised to assess the influence of possible errors of the ECMWF analyses in the failure of the 1981 warming event, as pointed out in Carton and Huang (1994). The wind stresses described in Servain et al. (1987) were the only other set of observations available as an alternative to the ECMWF wind stresses forcing. These wind stresses, produced from observations from 1964 to 1994 through subjective analysis, have an acceptable spatial coverage. Preliminary statistical analyses on them, shown the existence of a trend, that appears as the first component in an analysis of variance of the anomalies. But this trend practically disappears after 1980, which made the data set suitable as wind stress forcing during the last decade.

Unfortunately, the Servain et al. stresses cover only the tropical band, from 20°S to 30°N. The practical issue of including or not an anomalous forcing for the mid-latitudes, could not be separated from theoretical considerations. The importance of the forcing at mid-latitudes to simulate correctly the interannual variability of the equatorial Atlantic, was a point hard to decide in advance. Therefore, we have carried out two additional simulations of the ocean model, using anomalies of the Servain et al. stresses as forcing at the tropical band. In one of them, hereinafter referred to as S1, these anomalies are blended with the ECMWF anomalies, used in the rest of the domain. In the other, referred as S2, anomalous stresses cover only the tropical (from 20°S to 30°N) band and there is no anomalous wind forcing in the mid-latitudes.

The simulation of the GG index (dashed line) in run S1 is represented against the observations (thin line) in Fig. 12.2b. We can see an initial warming during 1980, that has no correspondence in the observations. The simulation of the 1981 warming is improved with respect to the run E1. The 1982 cooling is also simulated, while the 1984 warming occurs half a year earlier than in the observations. This warming event decays quite quickly, and afterwards an unrealistic cooling event

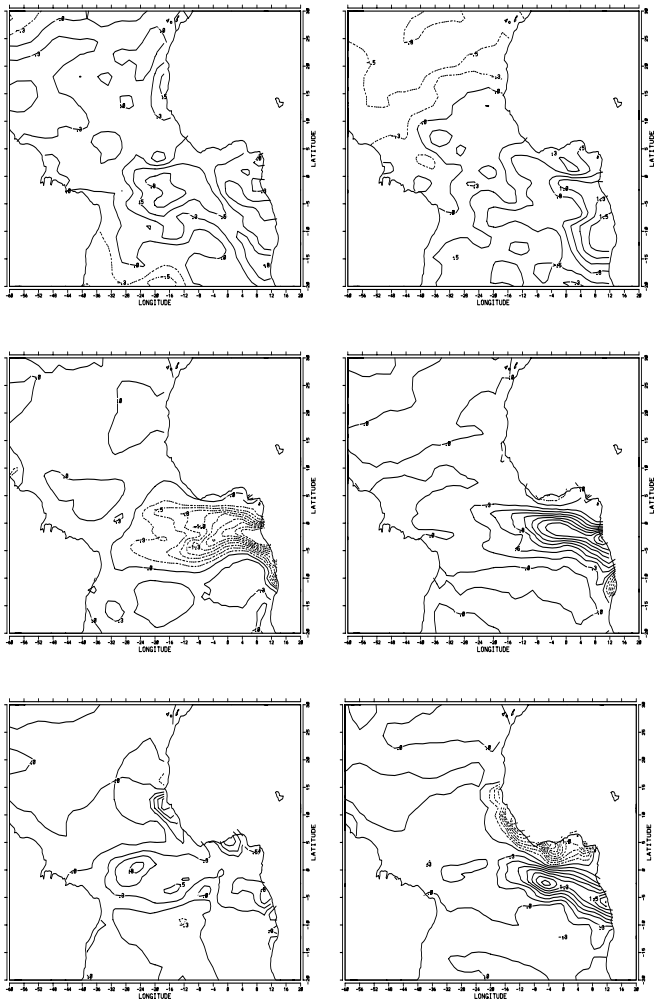

Fig. 12.3 Peak phase of the warmings of 1981 (right) and 1984 (left) from Servain data (top row), from the simulation E1 (middle row) and from the E2 (bottom row)

starts. Fig. 12.4 shows the SST simulation of the 1981 warming event (bottom left) and of the same stage of the 1984 event (bottom, right), in the run S1.

The GG index of run S2 represented in Fig. 12.2b with thick line, is not very different from the one of run S1. Values for the GG index during 1980 are closer to the observations than those of the S1 simulation. The magnitude of the 1981 warming is also underestimated. There on, the GG index of both simulations are almost indistinguishable. For the fourth simulation, referred as E2, the forcings were built by combining Servain climatology with the anomalous ECMWF stresses only in

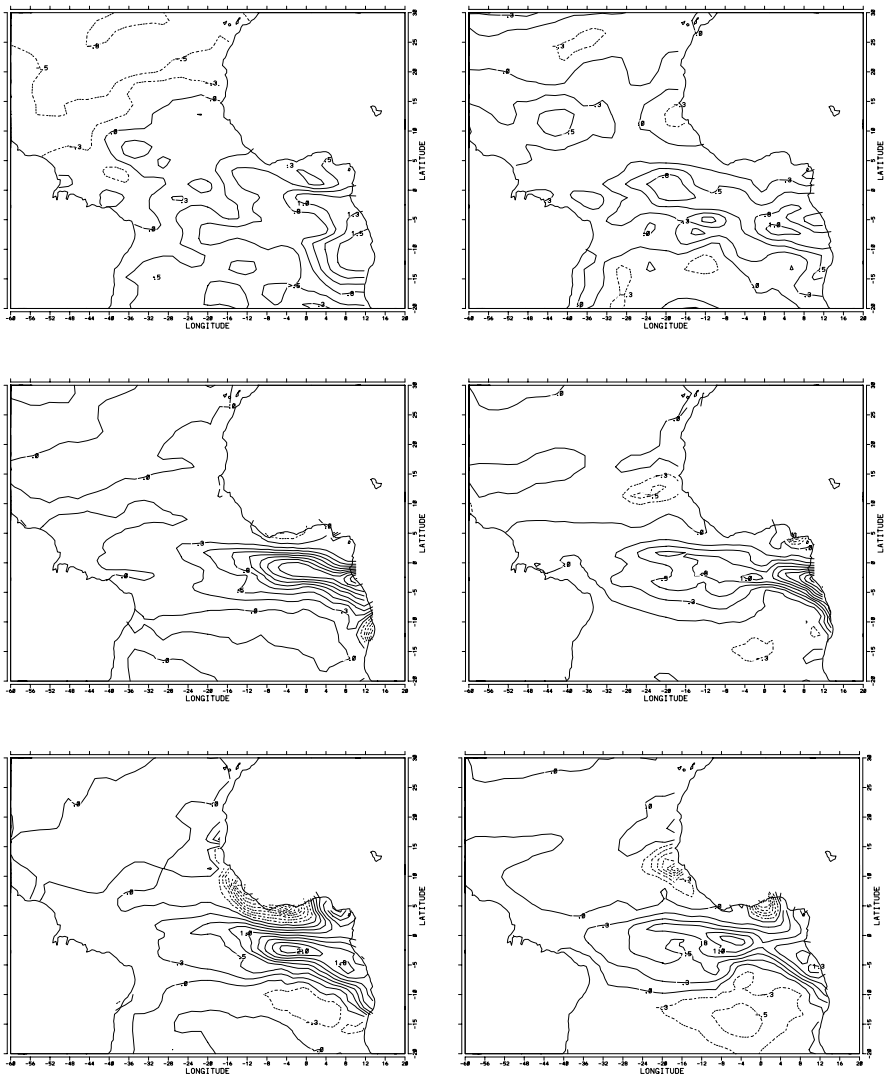

Fig. 12.4 Peak phase of the warmings of 1984 (right) and 1988 (left) from Servain data (top row), from the simulation E1 (middle row) and from the E2 (bottom row)

the tropical band. The GG index of run E2 is represented in Fig. 12.2a with a thick line and is very similar to the index of the run E1.

12.5 The tropical Atlantic variability in a coupled general circulation model.

To test the generality of some of the results obtained in the next section, we were allowed to analyze the interannual variability at the tropical Atlantic region that appear in 40 years of an extended global run with a coupled ocean-atmosphere general circulation model. The atmospheric component of this coupled run is the ECHAM4 general circulation model developed at Max Planck Institut fur Meteorologie (Hamburg). It is the current generation of ECHAM models which evolved under extensive reconstruction in parameterization, to adapt them to the needs of climate experiments. The model is run in a grid of approximately 2.8°. The oceanic component is the global version of the same oceanic model used here, the OPYC (Oberhuber, 1993). The scalar points of the oceanic model coincide with those of the atmospheric model except equatorward of 36, where the meridional grid is gradually decreased to reach 0.5° equatorward of 10°. The models are coupled quasi-synchronously, exchanging averaged quantities once a day. Details of this run can be found in Roeckner et al. (1996) or Bacher et al. (1997). For the purpose of comparison of the present paper we have analyzed a time slice of 40 years, from year 236 to year 275 of the present day climate simulation. The (filtered) GG index for this run is represented in Fig. 12.11 (middle row) with solid line. We see that the index presents traits of interannual variability that are common to the observed ones, albeit with reduced magnitude of the anomalies. The same can be said of the simulated Niño3 index (also filtered), represented in Fig. 12.11 (top row), also with solid line.

12.6 Statistical Comparison of the simulated interannual variability.

An useful variable to consider the start of the anomalous events is the heat content *hc* stored in the upper ocean at each horizontal grid point *(x, y)* and at each instant of time *t* as:

$$hc(t, x, y) = \rho c_p \int_{h_0}^{0} (T(t, x, y, z) - T_0(t, x, y))dz \qquad (12.1)$$

where $T_0(t, x, y)$ is the temperature at a reference depth h_0 = 360m and the same horizontal grid point and time *t*. It estimates the relative thermal energy stored in the upper ocean active layer. t

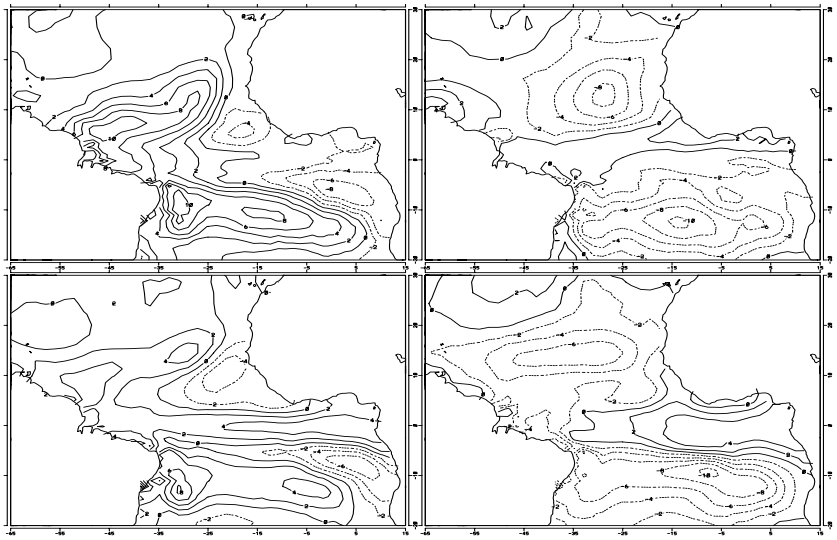

Fig. 12.5 Antecedent conditions (top) and initial stage (bottom) of the 1984 (left) and the 1988 warmings in the simulation E1.

In the ENSO case, changes of this variable anticipate the appearance of the anomalous SST (Chao and Philander, 1993). This feature is also present in our Atlantic simulation, as shown by Fig. 12.5 where the antecedent conditions to the 1984 and 1988 warmings are presented. In the case of the 1984 event (Fig. 12.5, left), antecedent conditions like the ones found for the ENSO case, are clearly identifiable in the previous autumn (above): there is a heat content accumulation in the western part of the basin, with centers north and south of the equator and a strong gradient along it. In the next season (winter 1984, below) the heat accumulation in the eastern equator referred by Huang et al (1995) as the initial stage of the events appears in a pattern hereinafter referred as “onset pattern”. There is no equivalent to the “antecedent pattern” in the seasons previous to the 1988 event (Fig. 12.5, right). Antecedent conditions of this event can be traced back as far as the spring of the preceding year, where warm water seems to accumulate at the eastern basin, while the heat content in the tropics is anomalously low. Just at the equatorial region, between 8° S and 8° N, this pattern has similarities with the “onset pattern” and therefore we will call it “preonset pattern”. Both conditions, “antecedent” and “preonset”, are traceable to anomalies of the currents, both outside and at the equator, that in turn are related with anomalies in the wind forcing. For instance in the autumn of the 83 there is a strengthening of the North Equatorial Current (NEC) and negative anomalies in the southern gyre while in the spring of 87 the situation is reverse: The anomalies of the currents in those two regions are positive. In both cases there are also important disturbances along the equator.

The characteristics of the simulated interannual variability can be summarized through a statistical analysis that captures the most relevant features of this variability in both, space and time. To this aim we use a version of the technique known as POP (Principal Oscillation Pattern) analysis (Storch et al., 1990). Propagating features can be better noticed in the POP analysis of the anomalous heat content. Anomalies of this field were built by subtracting the seasonal mean (the mean for each month) from the simulated value at the 15th of each month. The anomalous field was then smoothed, using a three points running mean average. Previous to the POP analysis, we proceed to the customary reduction of the degrees of freedom of the field by an expansion in terms of the Empirical Orthogonal Functions (EOF) of the field, and further truncation.

12.6.1 The simulations E1 and E2.

For the run E1, the four first EOFs retained explain 90% of the variance of the field. POP 2 shown in Fig. 12.6 (top left) is similar to the antecedent pattern we

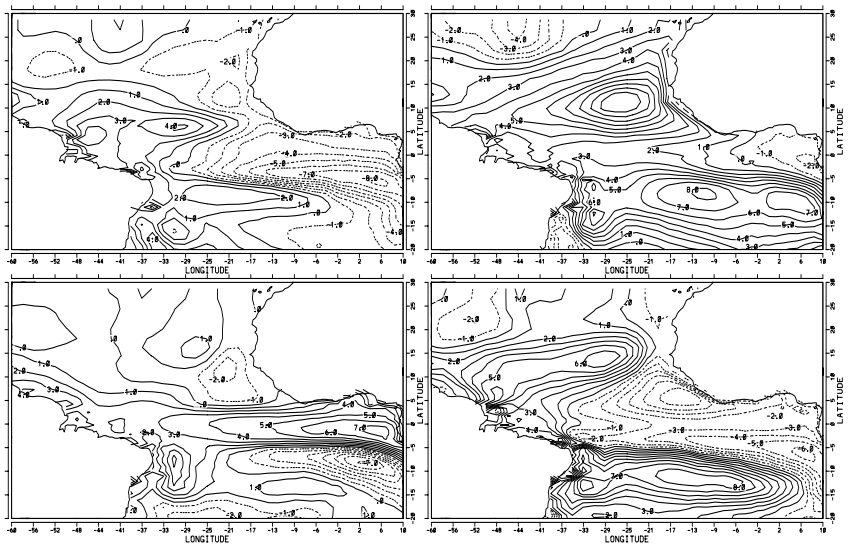

Fig. 12.6 Pair of POP 2/1 (left) and 3/4 (right) from the simulated heat content anomalies in run E1.

have discussed above while the POP 1, represented in the same figure, bottom left, correspond to the onset stage. Their time coefficients, shown in the top row of Fig. 12.7, compare well to the POP evolution scheme: P2 $\rightarrow$ P1 $\rightarrow$ –P2 $\rightarrow$ –P1. Maximum positive values in POP 2 precede the 1984 event by one year, and its maximum negative values yield the peak-mature stage of the episode. The POP 1 has maximum value in spring of 1984. The differences between the two warm

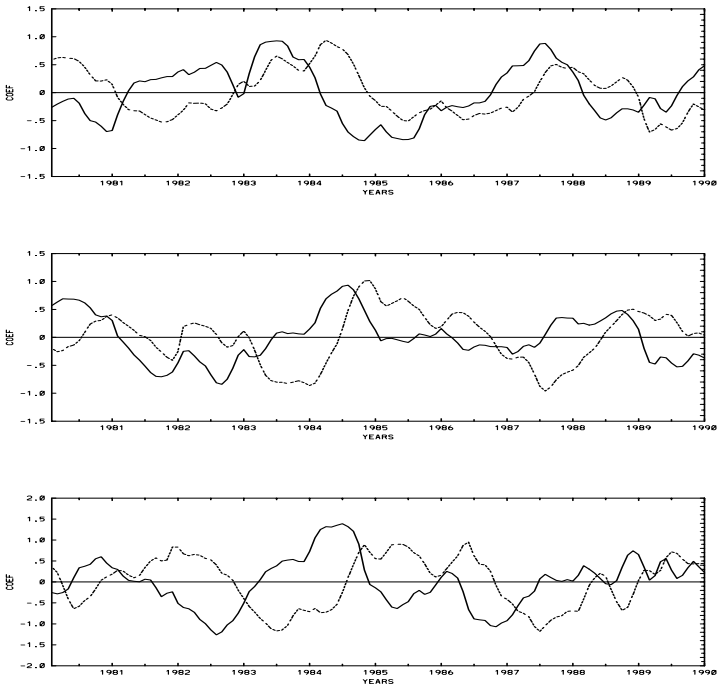

Fig. 12.7 Empirical time coefficients of the pair 1/2 of the POP of the simulated heat content anomalies in the run E1, E2 and S1. (top to bottom). (Time coefficient 1, solid line, time coefficient 2, dashed line)

events, 1984 and 1988, lie in the contribution of POP 3/4: while their coefficients (see top row of Fig. 12.8) have a different sign in the reconstruction of the 1984 event, they contribute with the same (negative) sign to the 1988 warming. It seems important at this point to remember that POPs belonging to different pairs are not orthogonal and therefore that the total variance explained by the two pairs cannot be obtained simply by adding the variance explained by each pair. Therefore, the contribution of each pair to the evolution of the anomalous heat content field has to be estimated in a less straightforward way. For this, three different anomalous heat content indices are built by averaging anomalies of the heat content through the same box used for the GG index. First, the anomalous heat content field is obtained from a reconstruction of the field with only the first four EOFs (10% of the variance of the field is then lost). This reconstructed field is identical to the one obtained with all four POPs. Second, the field is reconstructed with the pair of POPs 1/2, and last, the field is reconstructed with only the pair of POPs 3/4. Those are the indices represented in Fig. 12.10 (bottom row) with the short-dashed line, solid line, and long-dashed line, respectively. We can see from them how the evolution of the heat content in the region of interest is basically accounted for by the

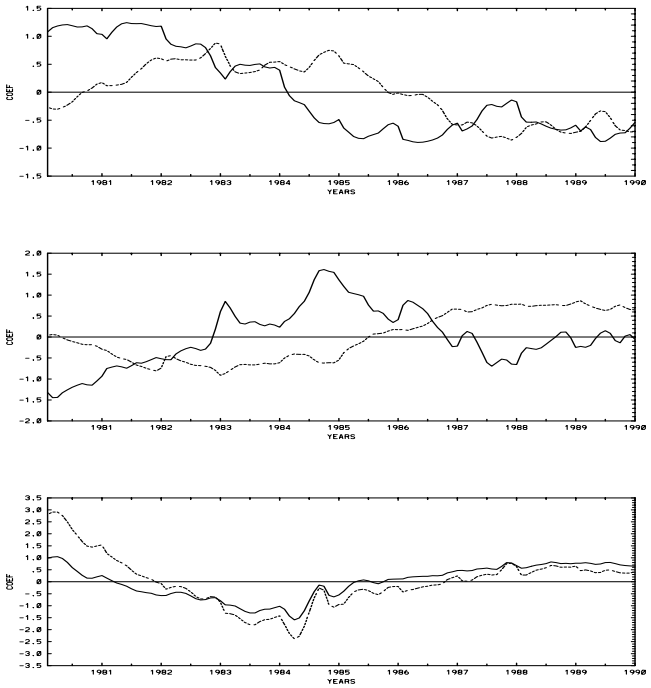

Fig. 12.8 Empirical time coefficients of the pair 3/4 of the POP of the simulated heat content anomalies in the run E1, E2 and S1. (top to bottom).

first pair of POPs. The second pair correct this picture, introducing the differences between the 1984 and 1988 events.

The POP time coefficients of the heat content anomalies of the run E2, shown in Fig. 12.10 and Fig. 12.11, middle rows, show similarity with those of run E1, and there is also a strong resemblance among the spatial patterns. But in this case, the contribution of the POP 1 is important also before the 1988 event and how the pair 3/4 contributes also to the reconstruction of the 1984 event.

12.6.2 Simulations S1 and S2.

In the case of the S1 run, the output is represented by the four first POP of the anomalous ocean heat content. The first pair of POP are represented in Fig. 12.9, and their evolution in time is plotted in Fig. 12.7 and Fig. 12.8 (bottom rows). Time coefficients of this conform well with the POP propagating scheme and the spatial patterns are similar to the first pair of patterns detected in the analysis of the E simulations.

12.6.3 The coupled ECHAM4/OPYC run.

The time series of the coupled simulation have, compared with the ones from the forced simulation, two peculiarities that are important from the statistical point of view: its length and the time sampling interval. Because we want to focus on common traits, we have chosen to project the anomalous heat content field of this simulation into the first pair of POP obtained in the analysis of the forced run E1. The patterns were interpolated to the grid of the coupled model, and the time series were previously filtered, to remove the variability associated to time scales lower than 18 months. The time evolution obtained for the POP 2 in this way is represented the Fig. 12.11 (top row) with dashed line against the Niño3 index of the coupled run (filtered), represented with solid line. The time coefficient of the projection onto POP 1 appear in the Fig. 12.11 (middle row) with dashed line against the GG index of the coupled run (filtered), represented with solid line. In this same figure we have represented an index for the anomalous heat content in GG (solid line), and the same index for a partial reconstruction of the heat content anomalous field in terms of the two patterns and the time coefficients obtained by projection.

12.6.4 Comparison of statistical relationships among variables

To model this relationship in the simplest way, we use a multivariate lagged regression. Let $s_j(t)$ be the time coefficient of the j-th POP of the heat content anomalies, and $r_k(t)$, the k-th principal component of some of the other simulated fields or of the forcing fields.

$$s_j(t) = \sum_{k=1}^{p} a_{jk}^{l} r_k(t-l) \qquad (12.2)$$

where l is a fixed time lag. The value of l is allowed to vary in a range from -6 to +6 months. For a certain j, to take into account a $r_m(t)$ and a lag l, two statistical tests have to be passed. Only the a_{jm} that are significantly different from 0 will be considered and in any case, the variance explained by the signal has to be greater than the residuals. For those regressions that passed both tests, we proceed to visual inspection. i

Next the anomalous fields of SST, mixed layer depth and mixed layer zonal and meridional velocities were expanded in terms of their EOFs. The first four principal components of each field, explaining an amount of variance from 60% (the mixed layer depth) to a 80% (SST anomalies), were combined (multivariate regression) to model the time coefficients of the four first POPs of the heat content. None of the selected fields was able to provide a satisfactory simulation of all the four time coefficients. The field that performed best was the meridional mixed layer velocity: the appearance of the warmings in the GG is due, in part, to an anomalous convergence of the meridional velocities in the mixed layer. An explanation for such relative failure can be the difference in the time scales of variability that we are trying to relate through the multivariate regression.

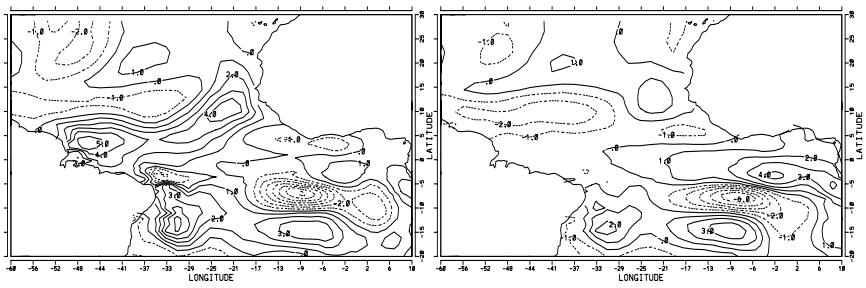

Fig. 12.9 Pair of POP 2/1 (left) from the simulated heat content anomalies in run S1

This lack of similarity is more evident between the forcing wind field and the output field (heat content). The forcing anomalies cannot even be reduced to a few modes. Therefore, we try to define for each grid point a variable that will measure its persistence rather than the forcing. Such variable is defined as

$$\theta_w = \int_{t-t_d}^{t} wc(\vec{r}_H, t')dt' \qquad (12.3)$$

where *wc* stands for the forcing variable (that is zonal or meridional wind or equivalently the wind stress curl and its divergence), $\vec{r}_H$ locates the grid point and t_d is the characteristic decorrelation time at $\vec{r}_H$. For each of these variables, seasonal anomalies were computed as usual. The anomalous values of the integrated forcing variables were then computed using expression (7.3).

We then proceed to a reduction of the number of degrees of freedom of the field through an expansion in terms of EOF. The variability of the forcing field used in the E1 run is well represented in terms of its six first EOFs, explaining from roughly 70% to 60% variance of the anomalies of the integrated wind fields.

When the regression of the $r_m(t\text{-}l)$ at *l* lag gives a satisfactory simulation of the $s_j(t)$, the regression coefficients allow for the identification of a spatial structure of the forcing whose temporal evolution gives an estimation of the heat contents with a certain lag. These patterns are known as associated patterns and are given by

$$\vec{v}_j = \sum_{k=1}^{p} a_{jk}^{l} \vec{e}_k^{l} \qquad (12.4)$$

where $\vec{v}_j$ is the atmospheric pattern associated to the *j-th* POP, $\vec{e}_k^{l}$ the k-th EOF, and a_{jk}^{l}, the coefficients determined in regression (7.3) at lag *l*.

The analysis was originally carried out with the wind forcing resolved in terms of wind stress divergence and its curl (Cabos et al., 1998). An example of the best fit of each of the POP time-coefficients, when the forcings are described in terms of the integrated divergence and curl, are presented in our Fig. 12.12, while the corre-

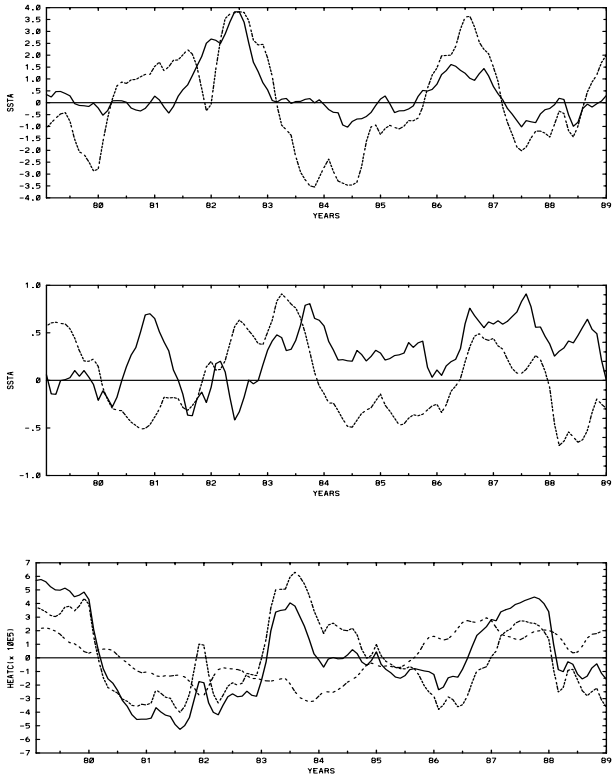

Fig. 12.10 Top panel, the observed Niño3 Index, filtered as to eliminate the variability associated to time scales lower than 18 months (solid line). Time coefficient the POP 2 of the first pair identified in the analysis of run E1 (dashed line). Middle panel, the observed GG Index filtered as above (solid line). Time coefficient of the POP 1 of the first pair identified in the analysis of run E1 (dashed line). Bottom panel, reconstruction of the GG Index of the anomalous heat content using the first pair of POP patterns and its time coefficients

sponding associated patterns are shown in Fig. 12.13. According to these last, the POP 1, 2 and 3 are preceded (lags -6 to -1) by extraequatorial signals in the Northern Hemisphere (north of 18° N) that maintain themselves for different lags.

In general, the multivariate lagged regression gives slightly better fit in the case of the integrated convergence. But there are cases, where both, the fit and the characteristics of the associated pattern of the integrated curl, are better (for instance, for the time coefficient of POP 3 in the E1 run). On the other hand, while the main signals in the first EOFs of the integrated convergence lie in the equatorial band, the first EOF of the integrated curl have important signals in the above mentioned region of the Northern Hemisphere. Therefore, a good fit in terms of the integrated curl indicates that the time evolution of this mode of the heat content is clearly determined by the extratropical signals in the wind forcing, and not merely the

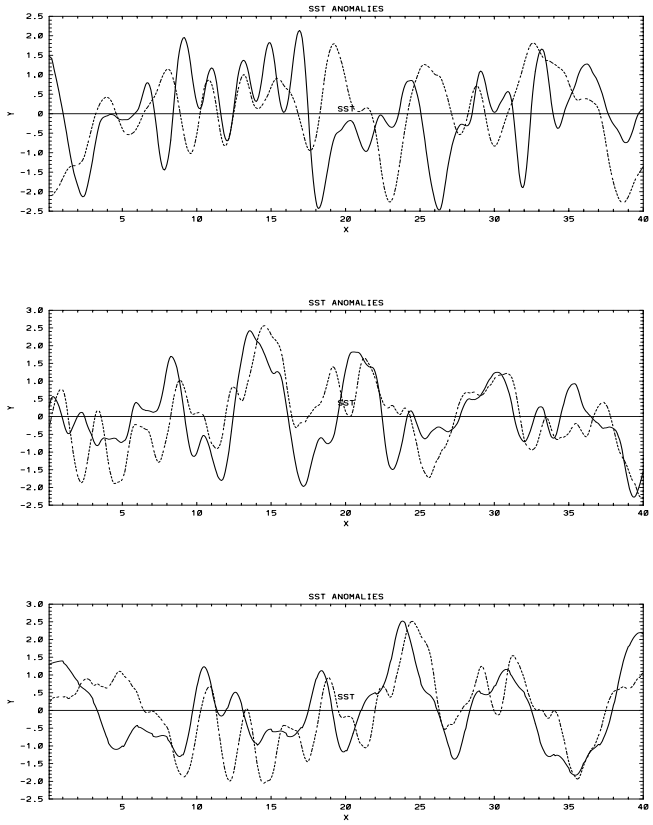

Fig. 12.11 Top panel, the simulated Niño3 Index of the coupled run, filtered as to eliminate the variability associated to time scales lower than 18 months (solid line). Time coefficient of the projection of the (filtered) anomalous heat content of the coupled run on the POP 2 of the first pair identified in the analysis of run E1 (dashed line). Middle panel, the simulated GG Index of the coupled run, filtered as above (solid line). Time coefficient of the projection of the (filtered) anomalous heat content of the coupled run on the POP 1 of the first pair identified in the analysis of run E1 (dashed line). Bottom panel, reconstruction of the anomalous heat content GG Index using the projection time coefficients and the two POP patterns.

result of the integration of the atmospheric noise in this region by the ocean model. In cases where both fields fit equally well the heat content time coefficient (as in POP 1/2), they allow for a complementary interpretation.

The extraequatorial signal that appear in the associated pattern 1 (the pattern associated to the evolution given by the time coefficient 1), centered in the Sargasso Sea, indicates sustained convergence. The associated signal in the integrated wind curl confirm the existence of a low pressure in this region. The extraequatorial signal in the associated pattern 2 is less clear and located in the middle Atlantic. The

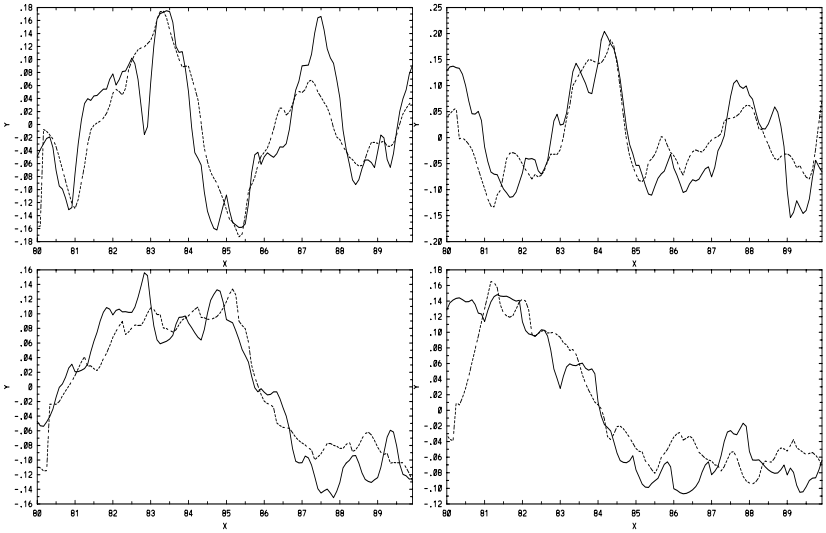

Fig. 12.12 Evolution of the empirical time coefficients of the POPs of the simulated anomalies of heat content (solid line) of the E1 run and fit obtained through multivariate lagged regression from the PC of the integrated forcing fields. Top left: the modeled time coefficient correspond to the POP 2 of the anomalous heat content, the forcing field is the windstress convergence, the optimal lag -2 month. Top right: the modeled time coefficient correspond to the POP 1 of the anomalous heat content, the forcing field is the windstress convergence, the optimal lag -4 months. Bottom right: the modeled time coefficient correspond to the POP 3 of the anomalous heat content, the forcing field is the windstress curl, the optimal lag -3 months. Bottom left: the modeled time coefficient is of the POP 4 of the anomalous heat content, the forcing field is the windstress divergence, the optimal lag -1 months.

signal in the associated pattern 3 is near the coast of Africa, weaker and noisier. The pair 1/2 of the associated patterns of the forcing fields in the S runs show similar signals in the subtropics and north of Bahamas (see Fig. 12.14).

Although all the associated patterns on both fields (convergence and curl) have important variability at the equator, the associated pattern obtained by fitting with the integrated divergence and curl, do not show any clear variability at the equator. Evolution from associated pattern 2 to 1 seems to be related to a persistent strengthening of the zonal winds at latitudes that coincide roughly with the maxima of the positive anomalies of heat content in POP 2 (see Fig. 12.6)

12.7 Discussion.

In the presented work we present several simulations of the interannual variability of the Tropical Atlantic for the decade 1980-1989, where three warming events

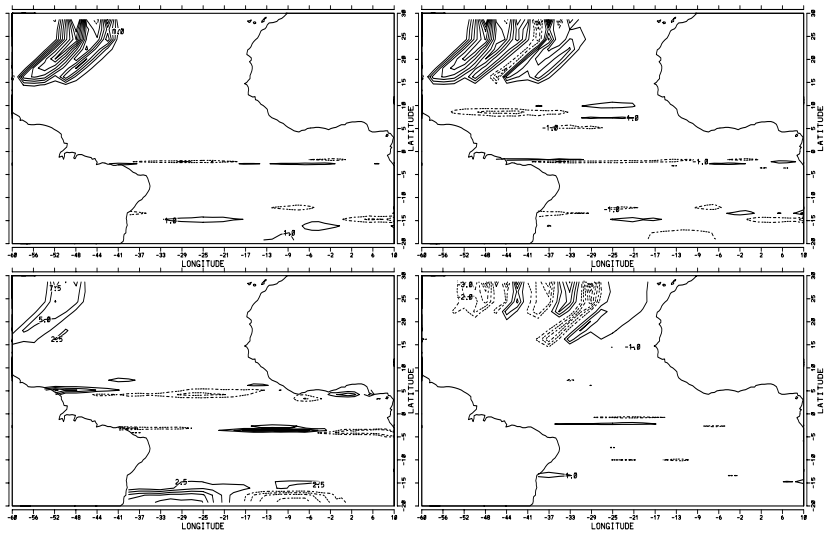

Fig. 12.13 Patterns of the integrated forcing field associated to the pair of POP 1(left top)/ 2 (right top) and to the pair of POP 3 (right bottom)/ 4(left bottom) of the anomalous heat content in the run E1.

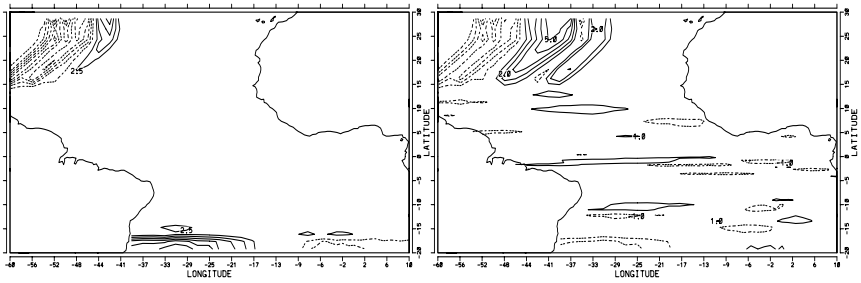

Fig. 12.14 Patterns of the integrated forcing field associated to the pair of POP 1(left)/ 2 (right) of the anomalous heat content in the run S1.

(1981, 1984 and 1988) where observed. The simulations could provide an exhaustive information (surface and subsurface) on the mechanism of generation of the events. Through their analysis, we want to understand the part played by the different oceanic mechanism and also by some characteristics of the forcings.

The simulations presented here were produced by forcing the same regional version of an ocean general circulation model with data sets built from observations, among these, the interannual anomalies of wind stresses. To simulate an acceptable annual cycle, most of the Atlantic domain had to be included. In the first of these simulations, where the anomalies of the ECMWF wind reanalysis were used for

the anomalous forcings, the performance of our model at simulating the variability at annual and interannual time scales is comparable to the one achieved by Huang et al.(1994,1995) using a very different (Cox's) model forced by the same wind stresses, although the resolution of our model is much coarser. Out of the 1981 event, both models reproduce quite well the warming and coolings of the period, somehow anticipated. And both overestimate the magnitude of the SST anomalies associated with the events.

The failure of both models at reproducing the 1981 warming might be due either to a trend in the ECMWF wind stresses or to the unrealistic (climatological) initial state of the anomalous run. To investigate this matter, another simulation was devised, with wind anomalous stresses built from observations of another data set (Servain et al. (1986)). In this new run, the 1981 event is more satisfactorily represented than in the first one. Two additional simulations, were performed to test the importance of including extraequatorial anomalies in the wind stresses.

Additionally, in order to check the results of our analysis, we will analyse also 40 years of the output of a global coupled simulation of the present day climate (ECHAM4/OPYC). The ocean model used for the forced simulations is the regional version of the oceanic component of the coupled run. Therefore, mechanisms of generation of the events that do not depend much on the atmospheric component are expected to be similar.

The generation of the events is best understood with the help of a variable that captures the thermal structure of the ocean, like the heat content. A statistical analysis of this field allows to reduce the number of variables to just only four patterns and their corresponding time coefficients. The first pair of modes shows propagating features, and together they give a representation of the events similar to the one found for the Pacific one: a redistribution of warm waters across the basin (Wyrtki, 1985). The second pair do not show propagating characteristics. The two first modes detected in our analysis give a reconstruction of the Gulf of Guinea index of the heat content that is more satisfactory in the case of the 1984 than in the 1988 event. To the reconstruction of this last, the contribution of the second pair of patterns is important.

On the other hand, the description of the events in terms of only four variables allow us to find easily a connection with ENSO. The pattern 2 of the first pair obtained from our statistical analysis of the two different forced runs, is the one that shows an accumulation of warm waters to both sides of the equator and negative anomalies at the gulf of Guinea. The time coefficient of this pattern in run E1, is represented in our Fig. 12.8 (top row). Its similarities with the observed Niño3 SST index, represented in the same figure, are evident. The warm SST anomalies in the equatorial Pacific, then, induce some changes that lead to increasing the heat content of the upper layers of the north tropical Atlantic, north of the equator. Because there is not a direct interaction between the two oceans, this feature suggest an atmospheric link. The time coefficient of POP 1, represented in Fig. 12.8 (middle row), is obviously related to the observed (SST) Gulf of Guinea index, also represented in the same figure. Nevertheless, out of the equator, the correction

made by the second pair of modes to the evolution given by the first one must be substantial. Snapshots of the heat content at stages previous to the appearance of the surface warmings, show that in the case of the 1988 event, the heat content is drained from the western part of the equatorial Atlantic, without been previously accumulated there. Our analysis of the anomalies of the heat content in the other forced run (where the anomalies of wind stress from Servain et al.(1986) were used to build the wind forcing) detect a first pair of pattern similar to the one found in the ECMWF run.

We have used the anomalous heat content field for the same domain in the coupled ECHAM4/OPYC3 run, to check the generality of the two first modes detected by our analysis of the forced run, and the connection of the second of these modes with Niño3 SST (Fig. 12.10). Propagating characteristics can be yet observed, and although the similarities between the second time coefficient and the simulated Niño3 index are here less evident, there are periods, as happened in the second decade, where both curves remain particularly close. It can be therefore concluded that the first pair of pattern detected by our analysis of the heat content field represent a mechanism of generation of the events that is quite frequent, although not the only one.

To explain the generation of the events, we try to relate, in a simple (linear) way, the anomalies of heat content to those of the surface variables and to the forcings. Only two of the four POP time coefficients that give the time evolution of the heat content anomalies can be expressed in terms of the principal components of surface variables (SST, mixed layer depth, u and v mixed layer velocity). Those fits point to the convergence of the meridional mixed layer velocity as one of the important mechanism that precedes the appearance of warm waters in the GG.

Due to the different time scales of variability, it is not possible to relate the anomalies of the heat content to those of the forcings using the simple multivariate lagged regression model. We define then some related to them that measure the persistence of the anomalies at each point of the grid. The evolution in time of these new fields is related to the heat contents through the linear model. The fitting of the POP time coefficients of heat content by the new atmospheric variables are quite good. Through regression coefficients, we determine four patterns of the forcing variables, whose time evolution match these of the POP of the anomalous heat content and that are associated to the time evolution of the POPs of the anomalous heat content.

In our analysis, the wind data were represented by its divergence and curl. The first pair of associated patterns show wavelike atmospheric activity at two narrow bands, north and south of the equator, at roughly the latitudes where the maxima of the heat content anomalies in the POP 2 are located. Persistent atmospheric anomalies in the northwest part of the basin are of relevance in the first three associated pattern. The evolution of the fourth POP is connected to a signal north of 18° N, near the coast of Africa. The extratropical signal is clearer in the pattern associated to the POP 2: the divergence and the curl pattern indicate a strengthening of the gyre near the northern boundary of the domain, with convergence south of it. In the

pattern associated to POP 1, the signal in the convergence field, weakened and noisier, has traveled eastward, toward the center of the basin and near the tropic.

Our analysis points, therefore, to two different ways in which warming events in the Atlantic can be generated. The first one is evident in the generation on the 1984 event, and is represented by the first pair of propagating patterns detected in the heat content field. The second POP, with an accumulation of heat content (warm waters) in the western part of the basin, north and south of the equator, and negative anomalies at the Gulf of Guinea, appears first. Its time evolution (very similar to the observed Niño3 index in the forced run and to the simulated Niño3 index for some time slices of the coupled run) suggest that this mode is forced by the Pacific warmings. Our statistical analysis detects extratropical atmospheric signals in the northern hemisphere that provide an interbasin link and can explain the anomalous heat content north of the equator. These atmospheric signals are centered at 20° N, 50° W, a region of downwelling, which strength is controlled by the wind curl, feed the subsurface tropical waters and influence through oceanic mechanisms the heat content at the equator. The first POP, representing the onset of the events, appear later and its evolution in time is well modelled by a convergence of mixed layer velocities at the GG that only in part is related to the atmospheric convergence. This first POP is connected also to an extratropical signal, located eastward of the one associated with the second POP.

By the second mechanism, warm waters accumulate slowly in the Gulf of Guinea and north of the equator, near the coast of Africa. In this last region, the accumulation is related to an anomalous atmospheric convergence. The transport by the countercurrent of these anomalies, slowly reinforces the Gulf of Guinea incipient warming and originates the warm event.

Acknowledgments. Thanks are due to J. Servain, that made his datasets available to us, and to the Laboratoire d' Oceanographie Dinamique et Meteorologie (LODYC) in Paris, for the FOQUAL-SEQUAL current measurements. The simulations reported in this paper were performed under contract EV5V-0124 and EV5V-CT94-0538C of the EC Environment Research Programme. Part of the computer time used was allotted at DKRZ(Hamburg) by the European Climate Computer Network (ECCN). When this time was exhausted, the Spanish Meteorological Office made additional CRAY hours available to us. The experiments with the S winds were supported by CRAY additional hours by the Spanish CICYT.

Finally, we are grateful to the Deutsches Klimarechenzentrum GmbH (DKRZ) for providing the output of the coupled experiments using the ECHAM4/OPYC3 model.